J Mater Sci (2009) 44:534–540
DOI 10.1007/s10853-008-3088-x

Structural, dielectric, and electrical studies on thermally evaporated CdTe thin films

S. Tewari · A. Bhattacharjee · P. P. Sahay

Received: 27 July 2008 / Accepted: 27 October 2008 / Published online: 23 November 2008
© Springer Science+Business Media, LLC 2008

Abstract Sandwich structures of cadmium telluride (CdTe) thin films between Ag electrodes were prepared by thermal evaporation technique at a vacuum of $\sim 2 \times 10^{-5}$ torr. Structural characterization of these thin films was performed using X-ray diffraction (XRD) studies. The effect of temperature and frequency on the electrical and dielectric properties of these films was studied in detail and reported in this article. The experimental study indicates that for the CdTe thin film the dielectric constant and dielectric loss increases with temperature and decreases with frequency. However, A.C. conductivity increases both with temperature and frequency. The data of complex impedance measurements over the same range of temperature and frequency are used to describe the relaxation behavior of the CdTe film. Our results indicate that the transport behavior of carriers in CdTe thin films is consistent with the correlated barrier hopping (CBH) model.

Introduction

Semiconducting thin films is an area of immense interest over the recent past, both in the field of academic research as well as in commercial applications because of their potential applications in optoelectronics devices. One very important series of such thin film semiconductors is the II–VI chalcogenides, which are well-suited for thin film optical devices owing to their large optical absorption coefficients and, also, they can be prepared in the form of high quality polycrystalline films from inexpensive raw materials by several methods [1–8]. Among the II–VI chalcogenide semiconductor thin films, the cadmium telluride (CdTe) thin films have drawn considerable interest owing to their wide range of use in optoelectronic and photovoltaic applications (like solar cells, IR and γ ray detectors, field effect transistors, etc.), particularly in the field of polycrystalline thin films. CdTe polycrystalline films have shown some promising potential for producing photovoltaic solar cells because of its high absorption coefficient (>10^{-4} cm$-^{1}$) and optimum band gap (1.5 eV) [1, 2, 5].

The CdTe thin films can be prepared by a variety of growth techniques [1–8]. Each of these reported methods has various advantages and disadvantages depending on the final application. In this article we report the studies carried out on CdTe thin films prepared by thermal evaporation.

The performance and efficiency of thin film-based devices are determined strongly by the electrical, dielectric, and optical properties of the component films. A study of these properties and their dependence on the film properties is very important as it helps in optimizing film parameters for better device applications. A.C. conductivity is an immensely important parameter, used to characterize the dielectric properties of materials. Measurement of A.C. conductivity of semiconductors has been extensively used to understand the transport mechanism in these materials [9–11] and to investigate the nature of defect centers, since they play a major role in the conduction process.

S. Tewari · A. Bhattacharjee (✉)
Department of Physics, National Institute of Technology, Silchar 788010, India
e-mail: ayonbh@gmail.com

P. P. Sahay
Department of Physics, Motilal Nehru National Institute of Technology, Allahabad 211 004, India

Impedance spectroscopy is an important analytical tool in materials research and characterization as the results may often be correlated with the complex microstructure of the materials [12].

There have been various models formulated [13–20], viz. the Quantum mechanical tunneling (QMT) [13, 14], small polaron tunneling model (SPTM) [15, 16], large polaron tunneling model (LPTM) [15], correlated barrier hopping (CBH) model [17–20], etc., to explain mechanisms responsible for A.C. conduction. The CBH model has been extensively applied to some chalcogenide semiconductors to explain the temperature-dependent properties.

Although the structural, electrical, and mechanical properties CdTe thin films have been studied by several groups [1–8, 21–24] in compounds as well as in other semiconductor thin films extensively, there is almost no report on the A.C. conductivity of CdTe thin films. In this present article we report the results of A.C. and D.C. conductivity measurements on thermally evaporated Ag/CdTe/Ag sandwich structured thin films. The temperature-dependent electrical conductivity and dielectric data has been analyzed with the aim of understanding the conduction mechanism.

Experimental

Sandwich structures of Ag/CdTe/Ag were produced on properly cleaned [25] glass substrates kept at room temperature using thermal evaporation technique in a vacuum of $\sim 2 \times 10^{-5}$ torr with a HINDHIVAC 12″ vacuum coating unit (model:12A4DM) using a Molybdenum boat as source holder and the deposition rate was kept constant at 3 Å/s. The thickness of the CdTe thin film was monitored in situ during the entire deposition process using a digital quartz crystal monitoring system (DTM: 101) and was found to be 2,850 Å. The thickness was reconfirmed using Tolansky's interferometric method with a CdTe film produced simultaneously and found to be correct with an error of $\sim \pm 2\%$. Using the hot probe experiment the CdTe films were found to exhibit n-type semiconducting behavior.

Silver electrodes are used as they provide ohmic contacts on CdTe. The work functions of Ag have been reported to be 4.44 eV [26] and the work functions of CdTe 5.9 eV [27], hence the condition to make Ohmic contact is satisfied. Silver electrodes of thickness 2,000 Å are deposited from a tungsten spiral at vacuum of $\sim 2 \times 10^{-5}$ torr at the rate of 2.5 Å/s. Using masks Ag/CdTe/Ag sandwich structures of area 7.163×10^{-06} m^2 were obtained.

X-ray diffraction (XRD) scans of the films were performed using a PANalytical X'pert Pro X-ray diffractometer applying the step scanning mode in the scanning angle range 20–80^0 with a step of 0.02^0 (2θ) and a counting time of 0.3 s for each step using Cu-Kα radiation with wavelength $\lambda = 1.54060$ Å. The X-ray source settings were 30 mA and 40 kV.

The dielectric properties like dielectric constant (ε_r) and loss tangent ($\tan\delta$) of the film are calculated from the A.C. measurements of impedance, capacitance, and phase angle, measured as function of frequency (10 Hz to 100 kHz) and temperature in the range 25–200 °C using HIOKI-LCR (Model:3522–50 Hioki, Japan) hi-tester, maintaining a vacuum of 10^{-2} mbar. The connections between the sandwich device and the LCR meter were made with coaxial cable. The temperature was monitored during entire experiment using a pre-calibrated chromel–alumel thermocouple with the help of Motwane digital multimeter (Model: 545). The resistivity measurements were conducted at different temperatures in the same temperature range, maintaining a vacuum of 10^{-2} mbar by two probe method using Keithley electrometer (Model: 6514). All the parameters were repeatedly measured using six different Ag/CdTe/Ag sandwiches and the data obtained was found to be highly reproducible.

Results and discussion

Structural analysis

The XRD data were analyzed using the X'pert High Score software. Qualitative phase analysis of each diffraction pattern was then carried out using the ICDD diffraction database and the search-match tool.

The XRD pattern shown in Fig. 1 for the CdTe film deposited, keeping the substrate at room temperature, presents a sharp diffraction peak at $2\theta = 23.7939^0$, which corresponds to (111) planes of the cubic CdTe structure. It confirms that in the CdTe film the microcrystallites have a preferential crystal plane orientation (111) parallel to the substrate. The crystallite size is calculated using Debye-Scherrer formula $D = \frac{K\lambda}{\beta \cos\theta}$ where, D is the crystallite size, λ the wavelength of X-ray, θ is Bragg's angle, K is the Scherrer Constant having a value of 0.9 in our case and β is the corrected FWHM for instrumental broadening. The grain size thus calculated is found to be of size 208.2 nm. The lattice strain was found to be 0.18%. Apart from this single peak, which is the signature peak for CdTe, no other significant peaks are visible in the XRD pattern. This may be as a result of a disordered and distributed arrangement of micro-crystallites. Our results on the dielectric studies also indicate such a trend.

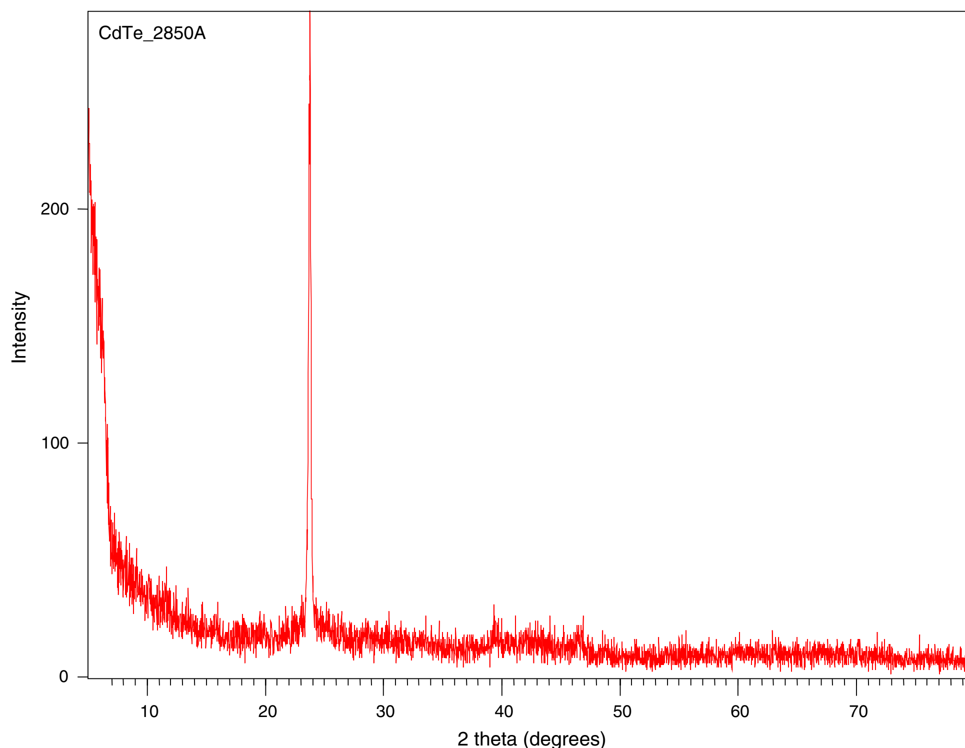

Fig. 1 XRD pattern of the CdTe film

D.C. conductivity

The D.C. conductivity is expressed by the relation,

$$\sigma = \sigma_0 \exp\left(\frac{-E}{kT}\right) \quad (1)$$

where σ_0 is pre-exponential factor depending on the nature of the sample, k is Boltzmann's constant and E is activation energy. The variation of D.C. conductivity (ln σ_{dc}) with inverse temperature (1,000/T) is shown in Fig. 2. The plot (ln σ_{dc} vs. 1,000/T) has linear components indicating that the conduction in the film is through thermally activated process in the temperature range (25–200 °C). Moreover, the plot clearly shows two slopes, indicating two activation energies in the two temperature ranges. The activation energies calculated from the slopes of the graph are 0.03 eV and 0.255 eV, respectively, in the low (25–100 °C) and high (125–200 °C) range of temperatures.

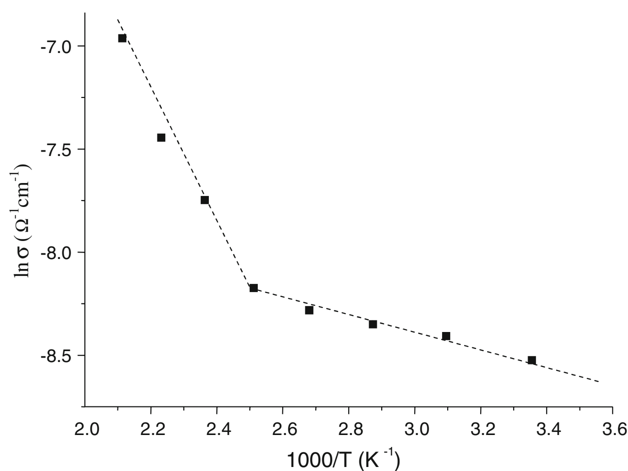

Fig. 2 Plot of lnσ_{dc} vs. 1,000/T

Dielectric properties

The variation of the dielectric properties like dielectric constant (ε_r) and dielectric loss tan δ with frequency for the CdTe thin film in the frequency range(10 Hz to 100 kHz) and temperature range (25–200 °C) for the Ag/CdTe/Ag sandwiched structure are shown in the Fig. 3a and b, respectively. The dielectric constant (ε_r) is found to decrease with increasing frequency for all the temperatures. Similar behavior is also observed for the variation of dielectric loss tanδ with frequency. This type of behavior suggests a distribution of relaxation times in the CdTe thin film system. The simple or complex defects that may be present in the film such as cracks, microvoids, imperfections, defect centers, etc., at sufficiently high concentration give rise to defect states, both shallow and deep states. These states may be of acceptor type (D^-/D^0) or donor type (D^0/D^+), or with three charge states as D^+, D^- and D^0 [28]. These defects immensely affect the transport properties of the materials by acting as traps and recombination centers for carriers and some D^+/D^- centers in close proximity form dipoles, which are responsible for the dielectric

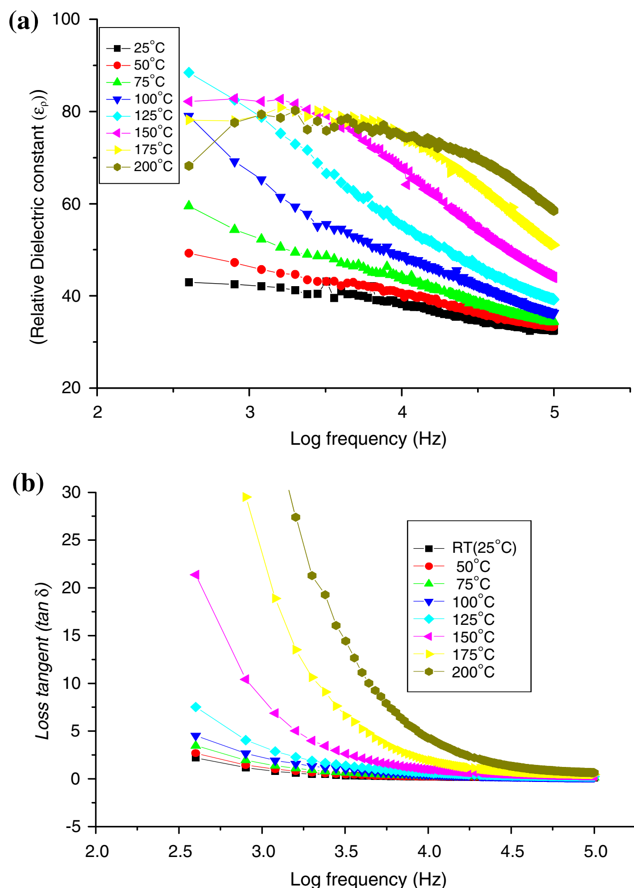

Fig. 3 **a** Variation of dielectric constant with frequency at different temperatures. **b** Variation of loss tangent with frequency at different temperatures

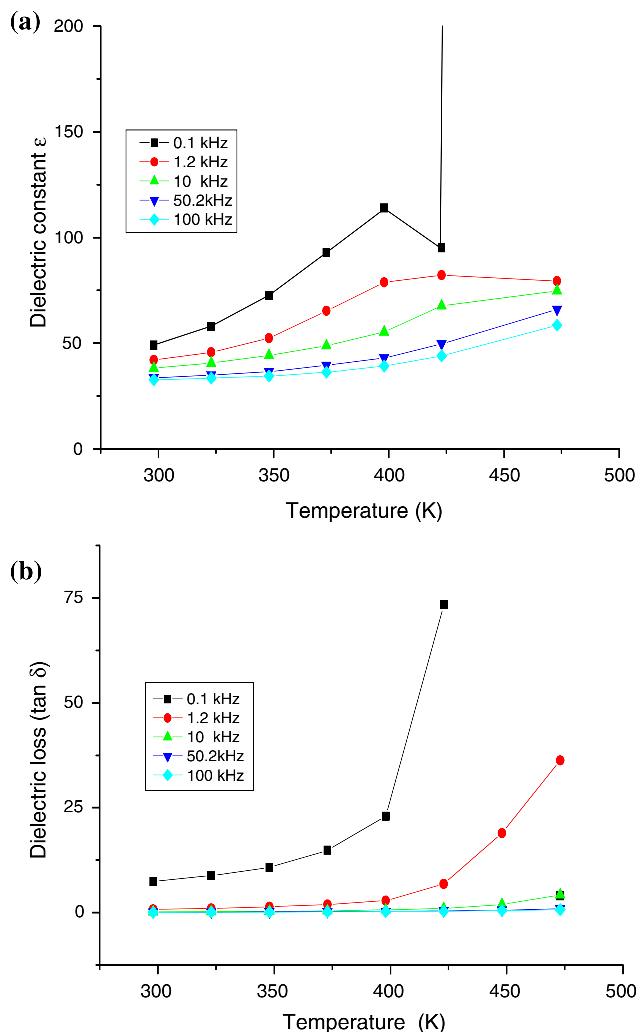

Fig. 4 **a** Variation of dielectric constant ε_r with temperature at different frequencies. **b** Variation of dielectric loss tanδ with temperature at different frequencies

behavior. From our structural studies we have estimated the grain size as 208.2 nm and found the system to be a considerably disordered one with only one intensity peak. Therefore, on subjecting the film to an electric field, the electrons hop between localized sites. The charge carriers moving between these sites hop from a donor to an acceptor state. Consequently, each pair of sites forms a dipole and contributes to the distributed dielectric relaxation.

The temperature dependence of ε_r and tanδ was investigated in the frequency range 10 Hz to100 kHz. Figure 4a and b shows the temperature variation of ε_r and tanδ at five different frequency ranges. It is observed that the dielectric constant ε_r slowly increases with rise of temperature and decreases with frequency. The dielectric loss tanδ is almost constant up to nearly 375 K and beyond that it increases with temperature. These observations may be related to the fact that at higher temperatures the loss is dominated by thermally activated hopping of carriers across the barrier. However, at lower temperatures the thermal activation is not so pronounced and the effect decreases considerably, resulting in no significant change of tanδ at lower temperatures.

A.C. conductivity

The A.C. conductivity is determined using the relation,

$$\sigma_{ac} = \varepsilon_r \varepsilon_0 \omega \tan \delta \quad (2)$$

and the corresponding activation energy is measured using relation

$$\sigma_{ac} = \sigma_0 \exp\left(\frac{-E_{ac}}{kT}\right) \quad (3)$$

where, σ_0 is pre-exponential factor, k is Boltzmann's constant and E_{ac} is activation energy on the measured data. Figure 5 shows the variation of A.C. conductivity with

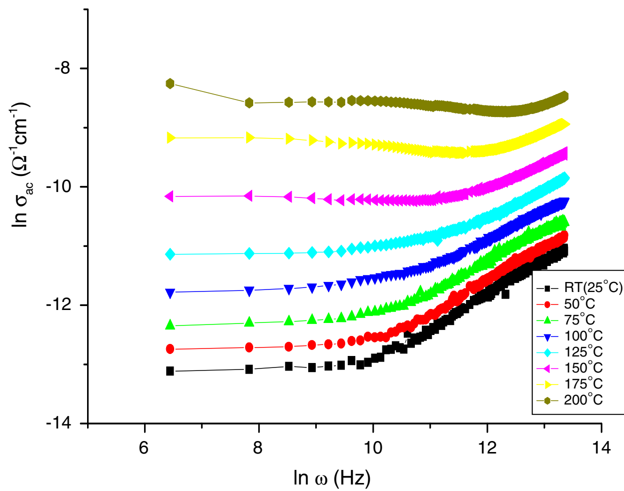

Fig. 5 Variation of A.C. conductivity with frequency at different temperatures

frequency (ln σ_{ac} vs. ln ω) in the temperature range temperature range 25–200 °C.

The frequency dependence of A.C. conductivity conductivity $\sigma_{ac}(\omega)$ obeys the relation

$$\sigma_{ac}(\omega) = A\omega^s \quad (4)$$

where A is a constant independent of frequency but dependent on temperature and ω is angular frequency, s is an index whose dependence on temperature determines the conduction mechanism in materials. In the CBH model s decreases with temperature whereas, for the small polaron model s increases with temperature.

It is evident from the Fig. 5 that the A.C. conductivity increases with the increase in frequency. This is a common occurrence and has been reported extensively for various other materials [29–31]. This type of variation is indicative of localized conduction where the A.C. conductivity increases with frequency. Contrary to this, in case of free

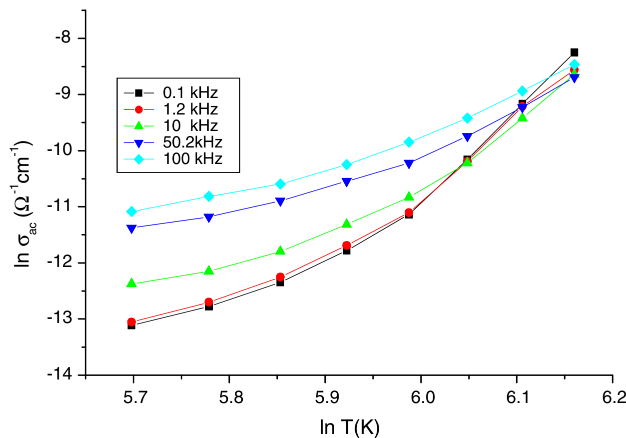

Fig. 6 Variation of A.C. conductivity with temperature at different frequencies

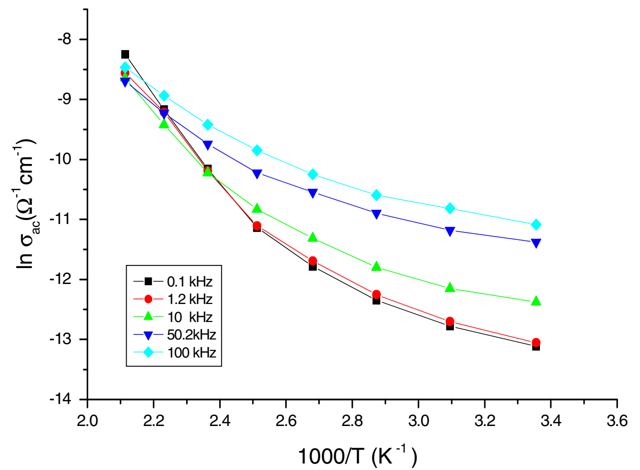

Fig. 7 Plot of lnσac vs. 1,000/T

band conduction the A.C. conductivity decreases with frequency [32]. Figure 6 shows the variation of A.C. conductivity with temperature. This clearly shows an increase in A.C. conductivity with increase in temperature. This rise of A.C. conductivity at higher temperature is due to thermal activation which allows the hopping of charged carriers between different localized states. This provides further evidence in support of the thermally activated conduction process that we have discussed in the section "Dielectric properties".

The variation of A.C. conductivity with inverse temperature (ln σ_{ac} vs. 1,000/T), is shown in Fig. 7. From the slopes of this graph the values of different activation energies are calculated as given in Table 1.

The exponent s in Eq. 4, is calculated from the slopes of Fig. 5, where we observe that the slope is different for higher frequencies (1 kHz to 100 kHz) and lower (10 Hz to 1 kHz) frequencies. Therefore, at each temperature we obtain two values of s, corresponding to the two frequency ranges. The values of s was found to be 0.113 for the lower frequency (10 Hz to 1 kHz) and 0.5668 for the higher (1 kHz to 100 kHz) frequency range. However, we observed that s increases with frequency but decreases with temperature. This trend was observed throughout the frequency range (10 Hz to 100 kHz). The observed variation of s (Fig. 8) in this investigation is in good agreement with

Table 1 Values of ac activation energies at different frequencies

Frequency (kHz)	E_1(eV)	E_2(eV)
0.01	0.6258317	0.167877
1.2	0.560368	0.172067888
10	0.4766408	0.133555538
50.2	0.33051	0.105964163
100	0.2994367	0.103975238

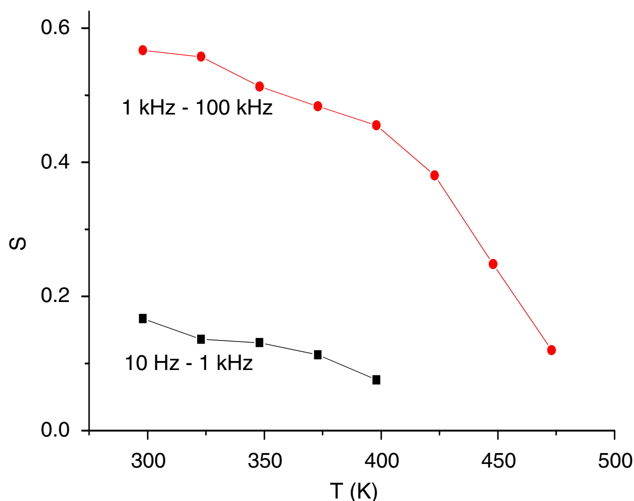

Fig. 8 Variation of frequency index s with temperature in two different frequency ranges

the observations reported elsewhere on semiconducting thin films [33] and it is in agreement with the CBH model [17–20]. Hence this model may be applied for explaining carrier transport mechanism in the CdTe thin films.

Impedance analysis

The Cole-Cole plots of the real and imaginary parts of Impedance Z′and Z″are shown in Fig. 9a and b over the studied frequency range 1 Hz to 1 kHz for the temperature ranges (25–100 °C) and (125–200 °C), respectively. The plots are found to be single semicircular arcs with their centers lying below the real axis at an angle θ. The finite value of the distribution parameter θ and a depressed arc are typical for material with multi relaxation processes [30]. The curves have non-zero intersection with real axis in the high frequency region and also, there is a decrease in the size of the plots with rise of temperature.

The observed behavior can be explained in accordance with an equivalent circuit model shown in Fig. 10 as similar to those proposed elsewhere [34]. A single arc is an indicative of single RC element [35], here the small resistance of value R_s is attributed to the core of CdTe grains while R_P and C_P are attributed to the grain boundary effect. The measured capacitance of such circuit is given by

$$C = C_P + \frac{1}{(\omega^2 C_P R_P^2)} \quad (5)$$

In this model the resistive element is assumed to vary with temperature according to the relation

$$R_P = R_0 \exp\left(\frac{-E}{kT}\right) \quad (6)$$

where R_0 is a constant and E is activation energy.

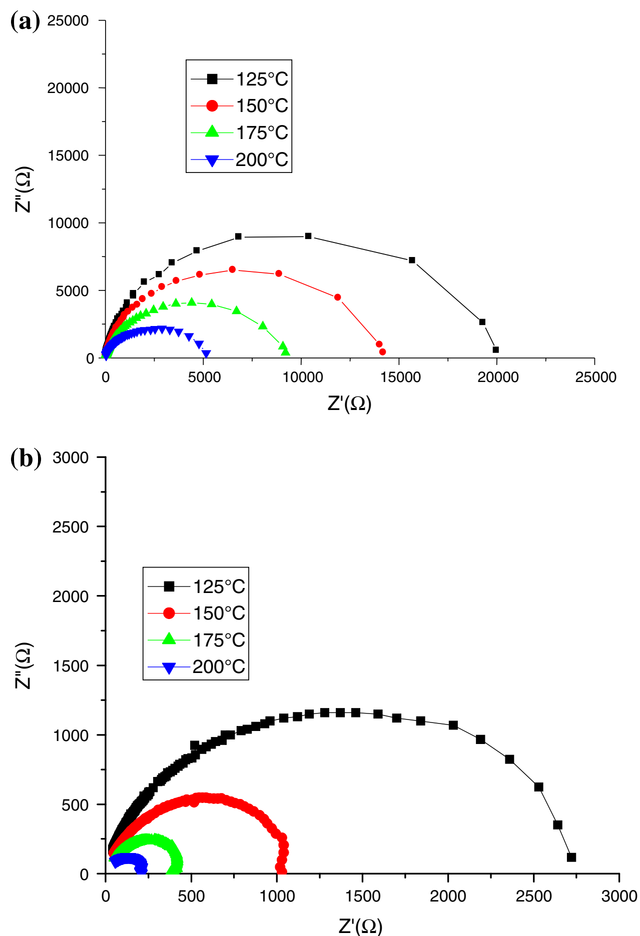

Fig. 9 **a** Cole-Cole plots in temperature range (25–100 °C). **b** Cole-Cole plots in temperature range (125–200 °C)

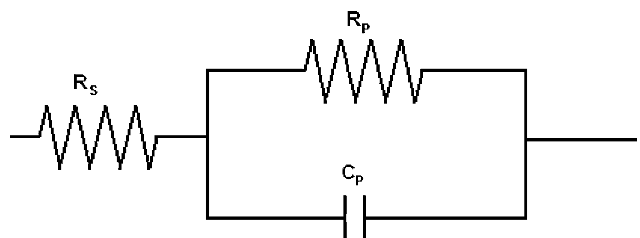

Fig. 10 R-C equivalent circuit model

In accordance with this equivalent circuit model the values of Z′and Z″are given by

$$Z' = R_S + \frac{R_P}{\left(1 + \omega^2 C_P^2 R_P^2\right)} \quad (7)$$

$$Z'' = \frac{-\omega C_P R_P^2}{\left(1 + \omega^2 C_P^2 R_P^2\right)} \quad (8)$$

These equations predict that the values of Z′and Z″ should decrease with increase in temperature which causes

shrinking of the Cole-Cole plots, as has been observed in our experiment.

Conclusion

Structural studies with XRD study revealed that the CdTe thin film material is of crystalline nature having (111) preferential orientation with crystallite size 208.2 nm. The D.C. conductivity of the film increases with temperature confirming typical semiconducting behavior and thermally activated conduction with different activation energies in different temperature ranges.

The dielectric properties such as dielectric constant and dielectric loss are strongly dependent on temperature and frequency and indicate a distributed relaxation. The nature of the A.C. conduction parameter s is found to decrease with temperature as per the theoretical prediction of the CBH model.

The Cole-Cole plots are found to be single semicircular arcs with non-zero intersection at the real axis and decreasing in size with rise of temperature indicating multiple relaxation processes.

Acknowledgement The author S. Tewari, acknowledges the financial support received from Council of Scientific and Industrial Research (CSIR), Government of India, New Delhi in the form of senior research fellowship (SRF).

References

1. Chu TL, Chu SS (1995) Solid State Electron 38:533
2. Chu TL, Chu SS (1993) Prog Photovolt 1:31
3. Kawai Y, Ema Y, Hayashi T (1987) Thin Solid Films 147:75
4. Takahashi M, Uosaki K, Kita H (1986) J Appl Phys 60:2046
5. Uda H (1993) In: Jain M (ed) II–VI semiconductor compounds, World Scientific, Singapore
6. Rusu M, Nicolaescu II, Rusu GG (2000) Appl Phys A 70:565
7. Hernandez-Contreras H, Contreras-Puente G, Aguilar-Hernandez J, Morales-Acevedo A, Vidal-Larramendi J, Vigil-Galan O (2002) Thin Solid Films 403:148
8. Ubale AU, Dhokne RJ, Chikhlikar PS, Sangawar VS, Kulkarni DK (2006) Bull Mater Sci 29:165
9. Elliott SR (1987) Adv Phys 36:135
10. Padmssuvarna R, Raghavendra Rao K, Subbarangaiah K (2002) Bull Mater Sci 25:647
11. El-Barry AMA, Atyia HE (2005) Physica B 368:1
12. Mcdonald JR, Johnson WB (2005) In: Barsoukov E, Mcdonald JR (eds) Impedance spectroscopy: theory, experiment and applications. Wiley-Interscience, NJ
13. Pollak M (1971) Philos Mag 23:519
14. Ghosh A (1990) Phys Rev B 42:5665
15. Pollak M, Pike GE (1972) Phys Rev Lett 28:1449
16. Lecleac HX (1979) J Phys 40:27
17. Elliott SR (1977) Philos Mag B 36:1291
18. Elliot SR (1978) Philos Mag B 36:129
19. Elliot SR (1978) Philos Mag B 37:135
20. Shimakawa K (1982) Philos Mag B 46:123
21. Mathewa X, Thompson GW, Singh VP, McClure JC, Velumani S, Mathews NR, Sebastian PJ (2003) Sol Energy Mater Sol Cells 76:293
22. Pandey RK, Mishra S, Tiwari S, Sahu P, Chandra BP (2000) Sol Energy Mater Sol Cells 60:59
23. Al-Shibani KM (2002) Physica B 322:390
24. Jacome CE, Florez JM, Gordillo G (2001) Thin Solid Films 396:255
25. Sahay PP, Nath RK, Tewari S (2007) Cryst Res Technol 42(3):275
26. Rhoderick EH (1978) Metal-semiconductor contacts. Clarendon Press, Oxford, p 54
27. Janik E, Triboulet R (1983) J Phys D Appl Phys 16:3
28. Prabakar K, Narayandass SK, Mangalaraj D (2002) Cryst Res Technol 37:1094
29. Gaffar MA, Abousehly AM, Abu El-Fadl A, Mostafa MM (2006) Cryst Res Technol 41:1120
30. Bhatangar VK, Bhatia KL (1990) J Non-Cryst Solids 119:214
31. Mardare D, Rusu GI (2004) J Optoelectron Adv Mater 6:333
32. Anwar M, Hogarth CA (1990) J Mater Sci 25:3906. doi: 10.1007/BF00582458
33. Suguna P, Mangalaraj D, Narayandass SAK, Meena P (1996) Phys Stat Sol (a) 155:405
34. Goswami A, Goswami AP (1973) Thin Solid Films 16:175
35. Andres-Verges M, West AR (1997) J Electroceram 1:125